

Static and swinging chemical waves in a two-interface dynamics on a ring

R. Sultan* and S. Jaafar

Department of Chemistry, American University of Beirut, Beirut, Lebanon.
E-mail: rsultan@aub.edu.lb

Received 9th August 1999, Accepted 22nd September 1999

An existing scaling model of a reaction–diffusion system is extended to a circular trajectory. The equations describe the evolution of a slow (X) and a fast (Y) concentration variable. The fast variable jumps between extreme values across a reaction interface as the rate parameter becomes very large. The model is reduced to one equation for the dynamics of the smooth (slow) variable while the Y -jumps occur at two interfaces spatially located on a ring. The equation is solved subject to 2π -periodicity conditions on the ring and continuity conditions at the interfaces. Both static (with zero velocity) and moving (with velocity v) wave solutions are found. An analogy is then drawn between our reaction–diffusion system and oscillating chemical reactions such as the Belousov–Zhabotinskii (BZ) reagent, confined to a torus-shaped container. A toroidal thin tube with a very small diameter could simulate the ring geometry. The conjectured waves capture the oscillations of the catalyst (ferroin), with the maxima and minima corresponding to the ferroin and ferriin, spatial domains in the doughnut, respectively. The non-stationary wave solutions predict a migration of those domains yielding swinging (back and forth) patterns along the ring. The azimuthal position of the interfaces exhibits temporal oscillations. Thus these simulations suggest interesting experiments on spatio–temporal patterns in excitable chemical media in annular reactors.

1 Introduction

Oscillating chemical reactions provide a beautiful example of a chemical wave phenomenon.^{1–3} Various known reagents act as media for the propagation of concentration waves of active chemical species far from equilibrium.⁴ The richest and most extensively studied chemical wave medium is the Belousov–Zhabotinskii (BZ) reaction.^{5,6} Both temporal oscillations and spatial structures are observed. The latter span a variety of fascinating features such as traveling waves, spiked profiles, target patterns, spirals, scrolls and static structures.

In the present study, we are interested in circular trajectories for the propagation of chemical waves, such as ones that would be triggered while confining the reaction medium to an annular gel-reactor, a uniform circular cavity or a torus-shaped container. Peculiar geometries for the propagation of chemical waves were considered in a variety of experiments, even spherical surfaces⁷ and narrow capillary tubes.⁸

The interest in wave propagation on circular trajectories triggered a number of studies, both experimental and theoretical (see Discussion). Spatio–temporal patterns on a ring geometry were observed in electrochemical^{9,10} systems. Rotating temperature pulses were IR-imaged in chemical reactions on ring-shaped metal catalytic surfaces.^{11,12} Stable Turing¹³ patterns were reported^{14,15} in the chlorite–iodide–malonic acid (CIMA) reagent system in an annular reactor with periodic boundary conditions. Periodic and chaotic oscillatory spatio–temporal patterns were obtained on a ring array of electrodes in sulfuric acid.¹⁶ Rotating “pinwheel” structures were painted¹⁷ on rings cut from cellulose nitrate or polysulfone membranes soaked with the BZ reagent.

We adopt a reaction–diffusion model developed earlier^{18–20} and adapt its equations to fit a circular geometry for wave propagation, as suggested by Ortoleva.²¹

2 Model

A two species reaction–diffusion system developed in refs. 18 and 19, involving a slow variable (X) and a fast variable (Y), was analysed using a “null velocity point” scaling technique yielding a scaled concentration X^* , given by:

$$X = X_0 + \varepsilon^{1/2} X^*, \quad (1)$$

where ε is an infinitesimal scaling parameter and X_0 the null velocity point. Under these conditions, the fast variable Y experiences jumps between the upper and lower branches of an S-shaped nullcline at constant X (Fig. 1) across a reaction interface $S = 0$. Let Y_0^I and Y_0^{II} be the values of Y on the lower and upper

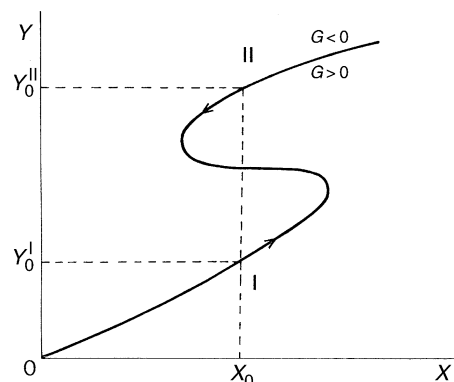


Fig. 1 Y -nullcline $G(X, Y) = 0$. As $\varepsilon \rightarrow 0$ [see eqn. (1)], the fast species Y experiences abrupt jumps at constant X between the values Y_0^I and Y_0^{II} on the lower and upper branches of the nullcline respectively. The arrows on the S-shaped curves show the direction of Y motion.

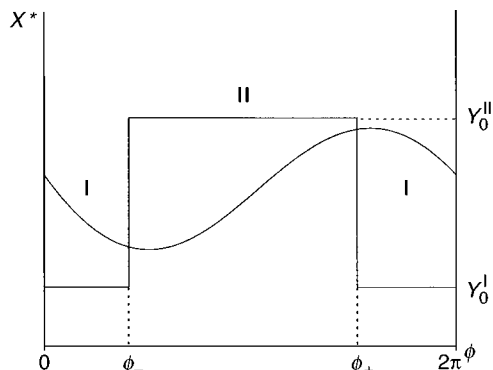


Fig. 2 A chemical wave on a circle “unfolded” into a linear axis, satisfying the periodicity conditions at $\phi = 0$ and $\phi = 2\pi$. The two interfaces are located at $\phi = \phi_-$ and ϕ_+ , wherein the continuity of X^* and $X^{* \prime}$ must be ensured.

and upper branches respectively. Then the reaction rate $f(X, Y)$ of the scaled slow variable X^* is shown to take either one of two fixed values F^I and F^{II} given by:

$$f(X, Y) = \begin{cases} F^I = f(X_0, Y_0^I) & S < 0 \\ F^{II} = f(X_0, Y_0^{II}) & S > 0 \end{cases} \quad (2)$$

With this, the reaction–diffusion equation describing the evolution of the scaled slow variable X^* takes the form:

$$\frac{\partial X^*}{\partial t} = D \nabla^2 X^* + \begin{cases} F^I & S < 0 \\ F^{II} & S > 0 \end{cases} \quad (3)$$

where D is the diffusion coefficient of X^* .

Eqn. (3) was solved in two-dimensional disk geometry yielding rotating spiral waves.¹⁹ Considered here in one dimension, it constitutes the starting point of the present study. Its solution is attempted on a ring where the Y -jumps occur at two positions in space across the reaction interface $S = 0$, as shown unfolded in Fig. 2. Let r_0 be the radius of the circular trajectory and ϕ denote the circular angle. Any spatial position x on the circular path is then determined by the length of the arc $x = r_0 \phi$ where ϕ is the swept angle. Since r_0 is a constant, the spatial coordinate is fully specified by a single variable, the angle ϕ . Call ϕ_- and ϕ_+ the values of ϕ (yet to be determined) at which the Y -discontinuities are located. Note that the continuity of the smooth variable X^* and its derivative must be ensured at ϕ_- and ϕ_+ (see Fig. 2).

Thus in the ring geometry, eqn. (3) becomes:

$$\frac{\partial X^*}{\partial t} = D \frac{\partial^2 X^*}{r_0^2 \partial \phi^2} + \begin{cases} F^{II} & \phi_- < \phi < \phi_+ \\ F^I & \text{otherwise} \end{cases} \quad (4)$$

This rearranges to the scaled equation:

$$\frac{\partial X^*}{\partial t} = \frac{\partial^2 X^*}{\partial \phi^2} + \begin{cases} f^{II} & \phi_- < \phi < \phi_+ \\ f^I & \text{otherwise} \end{cases} \quad (5)$$

where

$$f^I = \frac{r_0^2 F^I}{D}; \quad f^{II} = \frac{r_0^2 F^{II}}{D} \quad (6)$$

Thus in the present study we look for both static and moving wave solutions of eqn. (5) on the ring.

3 Static and swinging waves

3.1 Static waves

Because we are looking for static waves, we set $\partial X^*/\partial t$ in eqn. (5) equal to zero and thus obtain the equation:

$$\frac{d^2 X^*}{d\phi^2} + \begin{cases} f^{II} \\ f^I \end{cases} = 0 \quad (7)$$

This equation has the solution:

$$X^* = \begin{cases} X_1^* = -f^I \phi^2/2 + b\phi + a & 0 \leq \phi \leq \phi_- \\ X_2^* = -f^{II} \phi^2/2 + d\phi + c & \phi_- \leq \phi \leq \phi_+ \\ X_3^* = -f^I \phi^2/2 + f\phi + e & \phi_+ \leq \phi \leq 2\pi \end{cases} \quad (8)$$

This solution yields eight unknowns consisting of the six constants a, b, c, d, e and f augmented by the angles ϕ_- and ϕ_+ . We now find these constants by applying the following boundary and continuity conditions:

(i) 2π -periodicity for X^* and its derivative:

$$X_1^*(0) = X_3^*(2\pi) \quad (9)$$

$$X_1^{* \prime}(0) = X_3^{* \prime}(2\pi) \quad (10)$$

where a prime denotes a first derivative with respect to the variable ϕ .

(ii) Continuity of X^* and its derivative at ϕ_- :

$$X_1^*(\phi_-) = X_2^*(\phi_-) \quad (11)$$

$$X_1^{* \prime}(\phi_-) = X_2^{* \prime}(\phi_-) \quad (12)$$

(iii) Continuity of X^* and its derivative at ϕ_+ :

$$X_2^*(\phi_+) = X_3^*(\phi_+) \quad (13)$$

$$X_2^{* \prime}(\phi_+) = X_3^{* \prime}(\phi_+) \quad (14)$$

(iv) Eqns. (9)–(14) are augmented by the two conditions (see Fig. 2):

$$X_2^*(\phi_-) = -X_2^*(\phi_+) \quad (15)$$

$$X_2^{* \prime}(\phi_-) = -X_2^{* \prime}(\phi_+) \quad (16)$$

The solution of eqns. (9) through (16) should allow the determination of the six constants that appear in eqn. (8) in addition to the coordinates ϕ_- and ϕ_+ . A problem arises with the last two equations [(15) and (16)]. It can be shown that when conditions (12) and (14) are applied to the quadratic solutions (8), we automatically arrive at the realization:

$$X_2^{* \prime}(\phi_-) = -X_2^{* \prime}(\phi_+),$$

thus making condition (16) redundant. Similarly, it can be shown that when conditions (11) and (13) are applied to the solutions (8), we obtain:

$$X_2^*(\phi_-) = X_2^*(\phi_+). \quad (17)$$

This new equation coupled to condition (15) imposed on the static solutions leads to:

$$X_2^*(\phi_-) = X_2^*(\phi_+) = 0. \quad (18)$$

This yields a seventh condition on top of eqns. (9)–(14). We note here that because of the circular symmetry, any value of the angle ϕ marking the first interface (Fig. 2) is equivalent to any other value. Thus ϕ_- can be chosen arbitrarily. This completes the description of the problem by eliminating one unknown. We therefore see that the difficulty that arose from the quadratic form of the solutions is resolved by the symmetry and periodicity on the circular geometry. Note that this treatment (*i.e.* the arbitrary choice of ϕ_-) is not necessary in the non-stationary solutions as shall be demonstrated in the next subsection (3.2). Furthermore, although ϕ_- is selected arbitrarily, the angular difference between the two interfaces defined as $\delta = \phi_+ - \phi_-$ is determined by the dynamics of the problem. The length of the arc $\Delta = r_0 \delta$ represents the distance between the two interfaces (*i.e.* the width of the II-domain) on the ring.

Fig. 3 shows a plot of the static solution X^* vs. the variable ϕ along an unfolded linear axis. The varying width of the II-

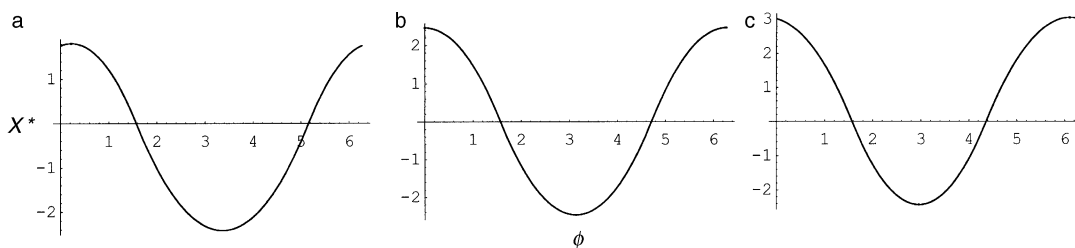


Fig. 3 Static waves obtained from eqn. (8) subject to the conditions of eqns. (9)–(16). Model parameters: $D = 1$; $r_0 = 2$; $F^I = +2$; a, $F^{II} = -1.5$; b, $F^{II} = -2$; c, $F^{II} = -2.5$. Note that the middle lobe (corresponding to the II-domain between ϕ_- and ϕ_+) becomes narrower as F^{II} becomes more negative at constant F^I .

domain seen in frames (a) through (c), is obtained as a result of the variation of one of the rate parameters (F^{II}). We see that the II-domain becomes narrower as F^{II} becomes more negative. This variation of the width δ of the II-domain with one of the rate parameters (F^{II} or F^I) while holding the other constant is depicted in Fig. 4. Note that δ decreases as F^{II} becomes more negative at constant F^I (frame a), while δ increases as F^I becomes more positive at constant F^{II} (frame b). It is also interesting to see that the two curves have different concavities. Thus the II-domain could either broaden or narrow down by an appropriate variation of the rate parameters F^I and/or F^{II} . Fig. 5 shows the static waves of Fig. 3 plotted on the ring. Fig. 6 shows a simulated “real-life” picture such as a BZ reaction medium in a thin torus-shaped container displaying grey level domains. The white color corresponds to the maximum value of X^* , while the dark grey (nearly black) color corresponds to the minimum value.

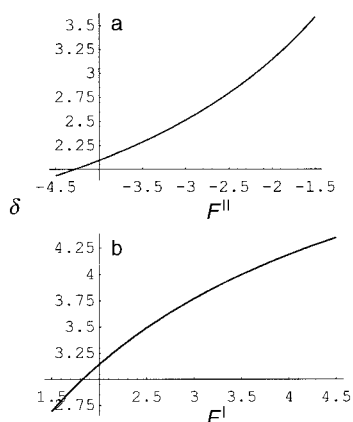


Fig. 4 Plot of $\delta = \phi_+ - \phi_-$ vs. the rate parameter F^{II} or F^I . Note that δ decreases as F^{II} becomes more negative at constant $F^I > 0$ (frame a) and increases as F^I becomes more positive at constant $F^{II} < 0$ (frame b).

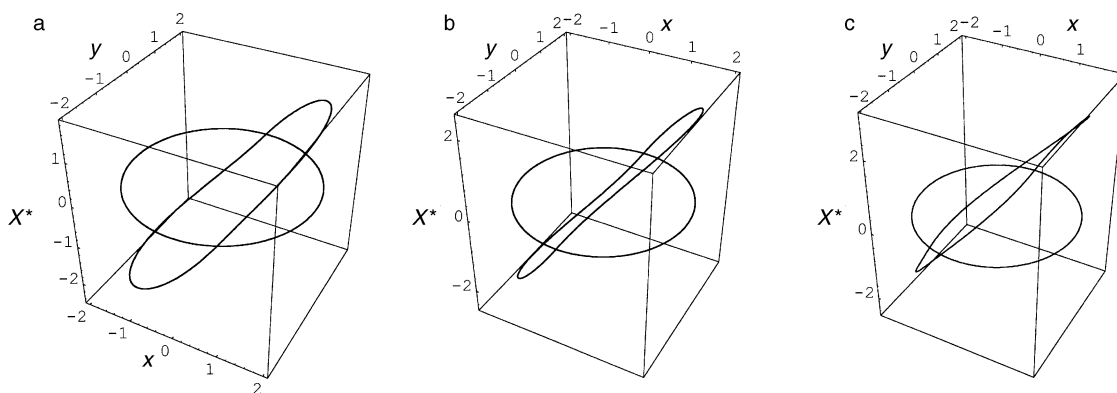


Fig. 5 Static waves plotted on the ring. The waves in frames a, b and c correspond to those on the linear axis in Fig. 3.

3.2 Swinging waves

We now look for propagating wave solutions on the ring. Let $\zeta = x - vt = r_0\phi - vt$ be a traveling wave coordinate. In this ζ coordinate frame, eqn. (5) becomes:

$$D \frac{d^2 X^*}{d\zeta^2} + v \frac{dX^*}{d\zeta} + f = 0, \quad (19)$$

where here:

$$f = \begin{cases} f^{II} & \phi_- < \phi < \phi_+ \\ f^I & \text{otherwise} \end{cases} \quad (20)$$

Eqn. (19) has the general solution:

$$X^* = c_2 e^{-v\zeta/D} - f\zeta/v + c_1. \quad (21)$$

Thus in the three regions of Fig. 2 we have:

$$X^* = \begin{cases} X_1^* = me^{-v\zeta/D} - f^I\zeta/v + n & 0 \leq \phi \leq \phi_- \\ X_2^* = pe^{-v\zeta/D} - f^{II}\zeta/v + q & \phi_- \leq \phi \leq \phi_+ \\ X_3^* = re^{-v\zeta/D} - f^I\zeta/v + s & \phi_+ \leq \phi \leq 2\pi \end{cases} \quad (22)$$

The periodicity conditions at 0 and 2π , along with the continuity conditions at $\zeta_- = r_0\phi_- - vt$ and $\zeta_+ = r_0\phi_+ - vt$ are applied in a similar manner as for the static solutions [eqns. (9)–(16)]. Note that because of the exponential term, the solution for the constants is obtained numerically. After the equations are solved at time $t = 0$, a time t_1 is chosen and the values of ζ_- and ζ_+ are determined for that time, then the evaluation continues at different time steps and so on. A time sequence for the moving wave on the unfolded (linear) axis is shown in Fig. 7. Fig. 8 displays the corresponding moving waves on the ring. Fig. 9 shows the time evolution of the hypothetical BZ reaction mixture in a thin toroidal tube (simulating 1D-annular geometry), displaying the migration of

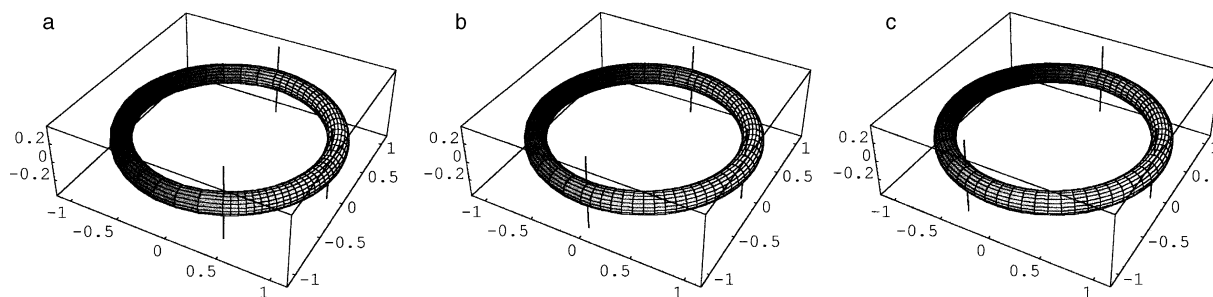


Fig. 6 Static waves in a BZ reaction medium confined to a torus with a thin cross section. The maximum in the wave corresponds to the white color (ferroin, in reality red), and the minimum corresponds to the black color (ferriin, in reality blue). The three vertical lines denote the positions $\phi = 0, \phi_-, \phi_+$. Note that as we go from frames a to c the grey domains (low X^*) shrink while the white region (high X^*) becomes larger.

the high concentration domains in either ferroin (white, maximum X^*) or ferriin (black, minimum X^*). Note that the real colors are red for ferroin and blue for ferriin. A very interesting result of this simulation is this back and forth (or

swinging) feature of the wave (Figs. 7–9), resulting from the temporal oscillation of the azimuthal angles ϕ_- and ϕ_+ , and subsequently the positions of the wave maximum and minimum. Such oscillations are depicted in Fig. 10. Note that

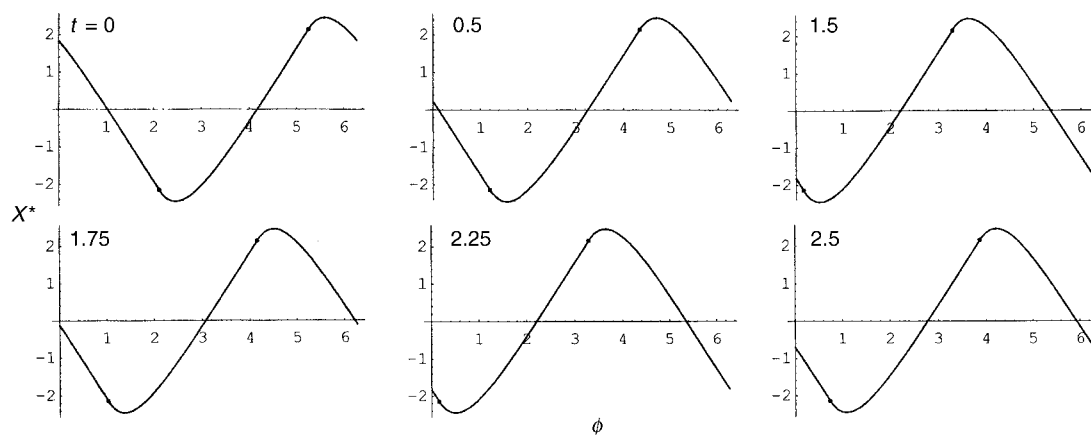


Fig. 7 Moving waves obtained from eqn. (21) subject to the conditions of eqns. (9)–(16). The ring here is unfolded into a linear axis. Model parameters: $D = 1; r_0 = 2; F^I = +2; F^{II} = -2; v = 1$; times $t = 0, 0.5, 1.5, 1.75, 2.25$ and 2.5 are indicated on the figure. The swinging character of these waves is seen notably in the sequence of times $1.5, 1.75, 2.25$ and 2.5 .

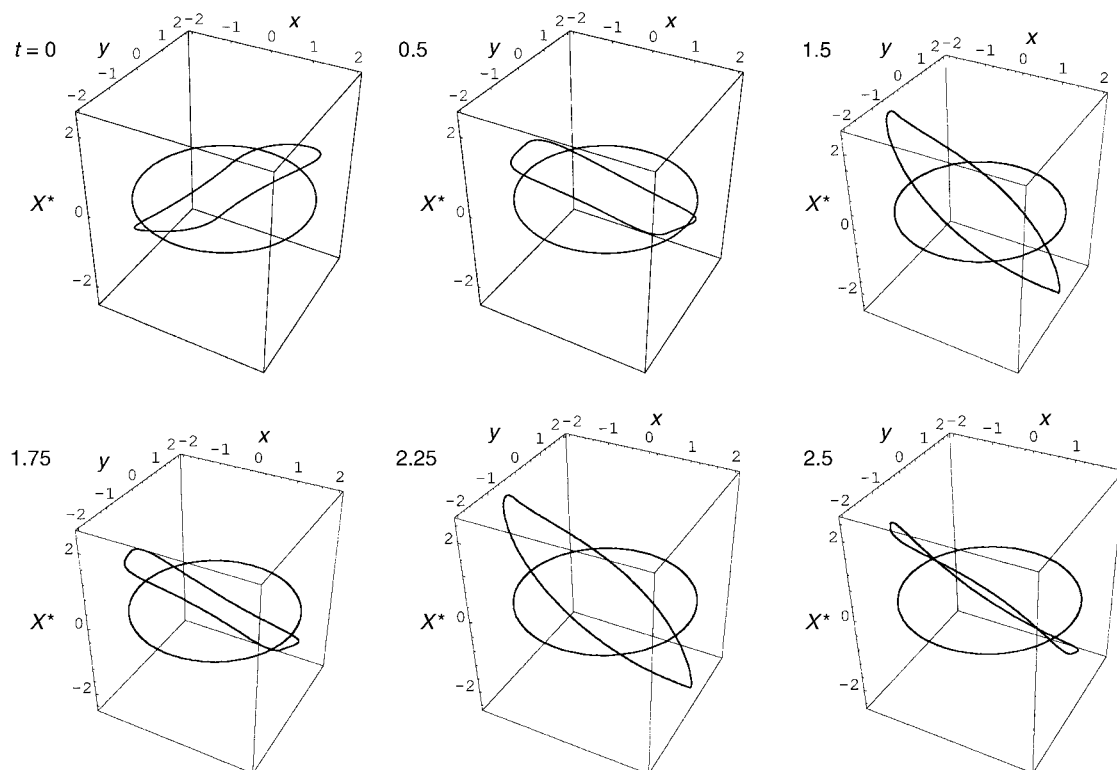


Fig. 8 The swinging waves of Fig. 7 plotted on the circular trajectory. The time evolution is indicated on the figure.

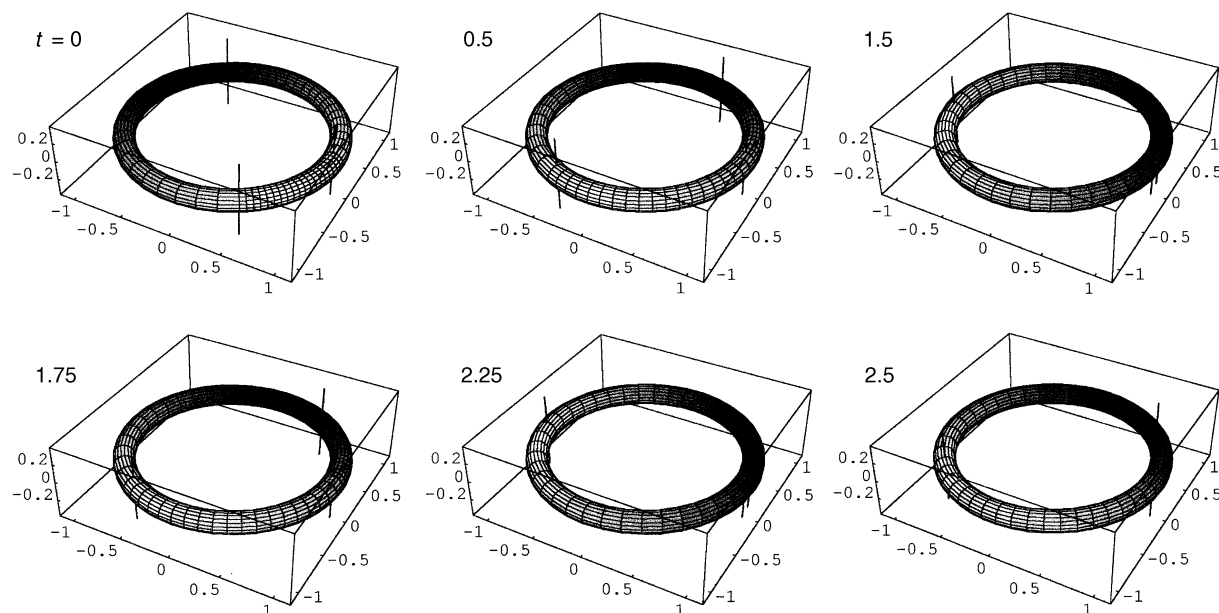


Fig. 9 Non-stationary concentration waves in a torus filled with BZ reagent, and their temporal circulation along the ring. The back and forth rotation of the black and white domains (seen notably in the sequence of times 1.5, 1.75, 2.25 and 2.5) suggests a swinging (or dancing) temporal pattern.

swinging pulses have been observed in a variety of physicochemical systems as documented in the Discussion.

4 Applications and discussion

This study presents a modeling of a reaction–diffusion system in a one-dimensional ring geometry. Stationary concentration waves consisting of opposite parabolas were found. Non-stationary (moving) wave solutions were also obtained involving a linear term and an exponential term. The moving waves display swinging (back and forth) oscillations of the various concentration domains in space. An important property of the obtained wave solutions is their stability. This feature is under present investigation and is the subject of a following paper. It actually appears that the stationary patterns of Section 3.1 are unstable leading to the moving waves. The swinging waves could thus emerge from the static patterns as the velocity bifurcates from zero. This scenario is yet to be verified.

The obtained results capture the features of previously observed oscillatory behavior in quasi-one-dimensional annular geometry. The propagation of rotating temperature pulses was observed during the oxidation of hydrogen on a nickel ring¹¹ and the oxidation of carbon monoxide on an

annular platinum thin film.¹² Infrared imaging “snapshots” show the time evolution of the pulse propagation over one period of rotation. The rotating and swinging T-domains resemble our white/black concentration domains. Swinging pulses that periodically change their direction of rotation around the ring were also reported²² as is conjectured here (Figs. 7–9). A wide variety of pulse patterns on a ring were simulated²³ using a simple cubic kinetic expression. Based on a FitzHugh–Nagumo²⁴ model, Nomura and Glass²⁵ demonstrated that excitable media can support a periodic wave of circulation on a one-dimensional ring trajectory. They obtained a reversal of rotation of the propagating pulse in a scenario whereby a right-going wave replaces an annihilated original left-going wave. They also showed that a left-going wave with two action potentials (double wave re-entry) replaces an original single pulse propagating to the left. Reversal of rotation of re-entrant waves and initiation of double wave re-entry were observed experimentally²⁶ in anisotropic rings of rabbit myocardium during entrainment of ventricular tachycardia. Fei *et al.*¹⁶ carried out experiments with a ring array of iron electrodes (all held at the same constant potential) in sulfuric acid. They obtained spatio-temporal current oscillations that range from unidirectional waves to anti-phase oscillations to chaos as the applied potential becomes more negative.

Of significant relevance and similarity to swinging waves are the so-called breathing patterns. Breathing pulses were conjectured²⁷ in a homogeneously oscillating chemical system subject to an initial disturbance. Using numerical simulations of an Oregonator²⁸ model, traveling fronts from opposite sides of a finite one-dimensional domain cause the quiescent region to contract and expand. Two-dimensional breathing patterns were demonstrated²⁹ in an open gel-disc reactor using the simulation of a reaction–diffusion system involving the Oregonator.

Another interesting feature of the present model is its generalizability to reaction–diffusion systems with more than just two interfaces. Such a development of the model is anticipated to yield rich structures with periodic alternations between red and blue (here white and black) domains of ferroin and ferriin respectively. It could perhaps explain the “pinwheel” structures of ref. 17. An elaborate version of this simple model is therefore worth exploring.

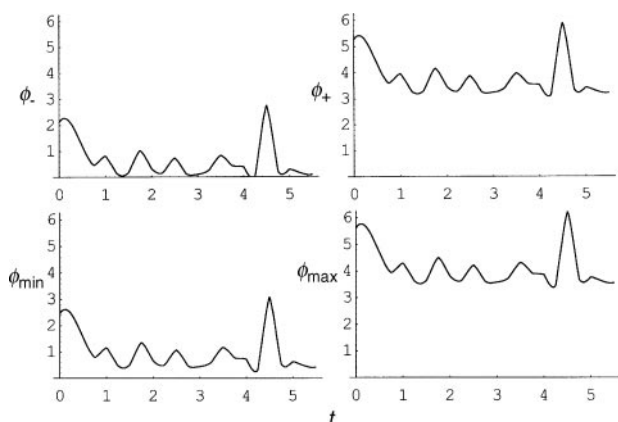


Fig. 10 Oscillations in the ring positions of ϕ_- , ϕ_+ , ϕ_{\max} and ϕ_{\min} with time, suggesting the swinging character of the moving waves.

Acknowledgements

This work was supported by a University Research Board (URB) grant No. DCU 17996071327, American University of Beirut.

References

- 1 *Chemical Waves and Patterns*, ed. R. Kapral and K. Showalter, Kluwer, Dordrecht, Netherlands, 1995.
- 2 P. Gray and S. K. Scott, *Chemical Oscillations and Instabilities*, Oxford University Press, Oxford, UK, 1990.
- 3 *Dissipative Structures and Chaos*, ed. H. Mori and Y. Kuramoto, Springer, Berlin, 1998.
- 4 G. Nicolis and I. Prigogine, *Self-Organization in Nonequilibrium Systems*, Wiley, New York, 1977.
- 5 *Oscillations and Traveling Waves in Chemical Systems*, ed. R. Field and M. Burger, Wiley, New York, 1985.
- 6 R. J. Field and F. W. Schneider, *J. Chem. Educ.*, 1989, **66**, 195.
- 7 J. Maselko and K. Showalter, *Nature*, 1989, **339**, 609.
- 8 Á. Tóth, V. Gáspár and K. Showalter, *J. Phys. Chem.*, 1994, **98**, 522.
- 9 O. Lev, M. Sheintuch and L. M. Yarnitzky, *Nature*, 1988, **336**, 458.
- 10 R. D. Otterstedt, P. J. Plath, N. I. Jaeger and J. L. Hudson, *J. Chem. Soc., Faraday Trans.*, 1996, **92**, 2933.
- 11 S. L. Lane and D. Luss, *Phys. Rev. Lett.*, 1993, **70**, 830.
- 12 S. Y. Yamamoto, C. M. Surko, M. B. Maple and R. K. Pina, *Phys. Rev. Lett.*, 1995, **74**, 4071.
- 13 A. M. Turing, *Philos. Trans. R. Soc. London, Ser. B*, 1952, **237**, 37.
- 14 V. Castets, E. Dulos, J. Boissonade and P. De Kepper, *Phys. Rev. Lett.*, 1990, **64**, 2953.
- 15 P. De Kepper, V. Castets, E. Dulos and J. Boissonade, *Physica D*, 1991, **49**, 161.
- 16 Z. Fei, B. J. Green and J. L. Hudson, *J. Phys. Chem. B*, 1999, **103**, 2178.
- 17 A. Lázár, Z. Noszticzius, H. Försterling and Z. Nagy-Ungvarai, *Physica D*, 1995, **84**, 112.
- 18 P. C. Fife, in *Nonequilibrium Dynamics in Chemical Systems*, ed. C. Vidal and A. Pacault, Springer, Berlin, 1984, p. 76.
- 19 R. Sultan and P. Ortoleva, *J. Chem. Phys.*, 1986, **84**, 6781.
- 20 R. Sultan and P. Ortoleva, *J. Chem. Phys.*, 1986, **85**, 5068.
- 21 P. J. Ortoleva, *Nonlinear Chemical Waves*, Wiley, Chichester, 1992.
- 22 H. Willebrand, T. Hüntler, F. J. Niedernostheide, R. Dohmen and H. G. Purwins, *Phys. Rev. A*, 1992, **45**, 8766.
- 23 U. Middy, D. Luss and M. Sheintuch, *J. Chem. Phys.*, 1994, **100**, 3568.
- 24 R. Fitzhugh, *Biophys. J.*, 1961, **1**, 445; J. S. Nagumo, S. Arimoto and S. Yoshizawa, *Proc. IRE*, 1962, **50**, 2061.
- 25 T. Nomura and L. Glass, *Phys. Rev. E*, 1996, **53**, 6353.
- 26 L. Boersma, J. Brugada, C. Kirchof and M. Alessie, *Circulation*, 1993, **88**, 1852.
- 27 A. L. Kawczyński, W. S. Comstock and R. J. Field, *Physica D*, 1992, **54**, 220.
- 28 R. J. Field and R. M. Noyes, *J. Chem. Phys.*, 1974, **60**, 1877.
- 29 J. D. Dockery and R. J. Field, *Phys. Rev. E*, 1998, **58**, 823.

Paper 9/06473G